LAWRENCE
LIVERMORE
NATIONAL
LABORATORY

LLNL-JRNL-651841

Quantifying Underestimates of Long-Term Upper-Ocean Warming

P. J. Durack, P. J. Gleckler, F. W. Landerer, K. E. Taylor

March 17, 2014

Nature Climate Change

Disclaimer

QUANTIFYING UNDERESTIMATES OF LONG-TERM UPPER-OCEAN WARMING

Paul J. Durack[1], Peter J. Gleckler[1], Felix W. Landerer[2] and Karl E. Taylor[1]

[1]Program for Climate Model Diagnosis and Intercomparison, Lawrence Livermore National Laboratory, Livermore, California, USA

[2]Jet Propulsion Laboratory, California Institute of Technology, Pasadena, California, USA

Submitted: Wednesday, 27 August 14
Abstract = 172 words
Main text = 2257 words
Methods text = 634 words
Figure legends text (words): Fig1 = 116; Fig2 = 76; Fig3 = 81; Fig4 = 102; Fig5 = 117
References = 30

Corresponding author address: Paul J. Durack, Program for Climate Model Diagnosis and Intercomparison, Lawrence Livermore National Laboratory, Mail Code L-103, Livermore, California, USA 94550.
E-mail: pauldurack@llnl.gov

The global ocean stores more than 90% of the heat associated with observed greenhouse-gas-attributed global warming[1-4]. Using satellite altimetry observations and a large suite of climate models, we conclude that observed estimates of 0-700 dbar global ocean warming since 1970 are likely biased low. This underestimation is attributed to poor sampling of the Southern Hemisphere, and limitations of the analysis methods that conservatively estimate temperature changes in data-sparse regions[5-7]. We find that the partitioning of Northern and Southern Hemispheric simulated sea surface height changes are consistent with precise altimeter observations, whereas the hemispheric partitioning of simulated upper-ocean warming is inconsistent with temperature observations. Relying on the close correspondence between hemispheric scale ocean heat content and steric changes, we adjust the poorly constrained Southern Hemisphere observed warming estimates so that hemispheric ratios are consistent with the broad range of modelled results. These adjustments yield large increases (2.2-7.1 x 10^{22} J 35yrs^{-1}) to current global upper-ocean heat content change estimates, and have important implications for sea-level, the planetary energy budget and climate sensitivity assessments.

Main

Numerous studies have examined the long-term (~1950-present) global mean and basin-scale evolution of ocean heat content (OHC) change in the upper 0-700 dbar[1,4,8-12] (See Supplementary Information) and important advancements have been made to correct for systematic measurement biases[6,13,14]. Evidence exists for a poleward shift of the subtropical gyres and marked warming in the Southern Ocean[7,15-17], but limitations of methods used to "infill" these data-sparse regions may introduce a conservative bias toward low magnitude (zero) changes[5-7]. Recent estimates of OHC change attempt to address sampling deficiencies by relying on coincident sea surface height (SSH) estimates or the modern Argo array[8,9,12,18]. Additional ocean warming studies apply formal detection and attribution approaches that rely on intrinsic variability estimates from models, and avoid using infilled data by "subsampling" models in space and time, consistent with the sparse historical observations[19-22].

Here, we investigate the large-scale spatial structure of heat content changes in five observational estimates (derived independently with differing processing choices) that were evaluated in the IPCC Fifth Assessment Report[4]. Based on a series of consistency checks with precise altimetry data and a large ensemble of climate models (Coupled Model Intercomparison Project phases 3 & 5), we find that observed Southern Hemisphere (SH) 0-700 dbar OHC changes are significantly underestimated. We analyse the 35-year period (1970-2004) over which both the CMIP5 "Historical" data are available and during which observational sampling deficiencies are small enough to yield reliable OHC changes, at least in the Northern Hemisphere (NH)[21].

OHC changes from the surface to 700 dbar are first examined in four observational estimates for which infilled gridded data were available[10,11,18,23] (Figure S2a; See Methods); A fifth dataset (Dom08[8]) provides only hemispheric timeseries, however is included in subsequent analyses below. In Figure 1a we show one of the observed results (Lev12[11]) alongside the CMIP5 Historical multi-model mean (MMM, Figure 1b). To facilitate comparison of the observed and simulated spatial structure of OHC changes, additional maps show results with the global average removed (Figure 1c, d; Figure S2a: A2-E2). The regions of inconsistency among the datasets are stippled, indicating where at least one of the four observational estimates disagrees in the sign of the mapped change (Figure 1a, c; Figure S2a: A1-D1, A2-D2), or where fewer than 75% of models agree with the MMM sign (Figure 1b, d; Figure S2a: E1, E2; Figure S2b: A2-D2, E2-I2). A prominent SH warming feature (30°S-50°S) is evident in MMM trend maps (Figure 1b, d; Figure S2b), consistent with previous modelling studies[24,25]. This strong warming is less distinct in all observational analyses (Figure S2a), which is likely due to SH data sparsity and internal variability that can mask the externally forced warming in this region. As expected, the MMM is smoother than the observed analyses because uncorrelated variability present in individual simulated records is averaged out (Figure S2a: A2-D2).

Oceanographic theory[26] and models[24,25] (Figure 1d, Figure S2b) suggest that shallow (above 700 dbar) ocean ventilation sites in the Southern Ocean (30-60°S) and the North Atlantic will warm at a faster rate than the global mean ocean. These patterns are broadly compatible with ocean ventilation proxies, diagnosed from anthropogenic CFC-11 tracer concentrations in the observed ocean and are well

87 replicated by a limited CMIP5 model subset (Figure S3; see Supplementary
88 Information).
89 Observational estimates of OHC are not completely independent as they
90 share data sources and in some cases apply similar processing procedures. The
91 Ish09[10] and Lev12[11] (Figure S2a: B1/2 & C1/2) datasets rely on similar objective
92 analysis methods and data sources (including XBTs, which require non-trivial bias
93 corrections), and both show a weak SH warming (compared to the NH), but a strong
94 North Atlantic warming. These features are also present, though smaller in
95 magnitude in the Smi07[23] result (Figure S2a: A1/2), which uses the covariance field
96 obtained from the HadCM3 model to infill gaps in data sparse areas (see
97 Supplementary Information). The DW10[18] analysis, which is based on a smaller
98 dataset of more accurate hydrographic measurements (excluding XBTs), suggests a
99 more homogeneous warming, with larger magnitudes in the South Pacific and South
100 Atlantic basins compared to the other analyses (Figure S2a: D1/2). In each of the four
101 observed analyses, the Atlantic basin is warming at a faster rate than the Pacific,
102 with the largest values found in the well-sampled North Atlantic, a feature also
103 apparent in the CMIP ensembles (Figure 1b, d; Figure S2b).
104 Although internal variability could explain a large portion of the discrepancy
105 between the observed and modelled estimates of OHC change (see Supplementary
106 Information), contributions from systematic model or observational errors are also
107 possible. To investigate the influence of such biases, and to test the physical
108 consistency of model simulations, we compare simulated changes in sea surface
109 height (SSH) to satellite altimetry measurements (see Supplementary Information).
110 SSH reflects ocean changes driven by steric expansion as the oceans warm

111 (accounting for approximately 40% of the long-term mean SSH change[27]), along with
112 mass contributions from the cryosphere, halosteric effects from regional salinity
113 changes and dynamic adjustments related to circulation changes. In models where
114 glacial melt waters are not represented, SSH changes on hemispheric scales are
115 almost entirely determined by full-depth steric changes, which are dominated by the
116 thermal component and therefore closely related to OHC changes (Figure 2, Figure
117 S4). Although the correspondence between simulated global mean SSH and OHC is
118 larger when the full ocean depth is considered (Figure 2d), the strong correlation
119 persists for the more variable upper-ocean (0-700 dbar; Figure 2a). The close
120 correspondence between OHC and SSH changes also holds at hemispheric scales
121 (Figure 2b-f), indicating that the better observed steric anomalies can be used as a
122 proxy for the hemispheric partitioning of OHC change. A number of studies have
123 relied on this relationship, and have used observed SSH to inform infilling
124 approaches for the sparse temperature observations[8,28] or estimate sampling
125 uncertainties[9,12] (see Supplementary Information). The key benefit of SSH data is
126 that contrary to poorly sampled in-situ temperature, satellite altimetry data cover
127 most of the globe and are sufficiently accurate to monitor changes since 1992.
128 We now contrast changes between the NH and SH by examining ratios of SH
129 versus global changes for both OHC and SSH (see Methods). This approach allows us
130 to effectively calibrate in-situ temperature results between the relatively well
131 sampled NH and poorly sampled SH.
132 We compare hemispheric ratios of SSH to their OHC counterparts considering
133 linear trends over successively longer time scales. For the observed and simulated
134 OHC changes we begin trend calculations in 1970, whereas for the observed SSH

135 data we begin in 1993 (Figure 3a, b). As expected, hemispheric trend ratios are noisy
136 on decadal or shorter time scales due to significant interannual variability; However
137 by 1990 (20-year trends) they have largely converged (Figure 3a, b).
138 We also perform a similar analysis for the truncated time period (1993-
139 present; Figure 3c, d). Independent of the starting date, the observed SSH estimate
140 lies well within the range of inter-model ratios for the CMIP5 Historical simulations
141 (0.68; Figure 3a MMM 0.62 vs inter-model standard deviation 0.50-0.73; Figure 3c
142 MMM 0.57 vs 0.45-0.69). In contrast, the trends in the observed OHC ratio appear to
143 be substantially smaller than simulated by most models, although they converge in
144 recent years. The consistency between the observed and simulated SSH ratios
145 suggests that the observed OHC discrepancy arises from SH sampling errors rather
146 than from model biases.
147 All but one of the four observational OHC trend estimates in Figure 3b
148 suggest a much smaller SH contribution, with stabilised ratios at time scales of 15-
149 years and longer, well outside the inter-model standard deviation (0.50-0.63, MMM
150 0.56 vs 0.33-0.49 for observations). With a 1993 start date (Figure 3d), the OHC
151 MMM trends stabilise within 10 years, whereas the observational OHC ratios
152 become progressively larger and trend toward better agreement with the modelled
153 estimates (MMM 0.53 and inter-model standard deviation 0.45-0.61 Figure 3d). This
154 shift in the observed OHC trend is consistent with an increasing influence of Argo
155 data after 2004, at which point in-situ measurements begin to provide near-global
156 coverage[29]. Therefore observational trend ratios become more consistent with the
157 models as the SH data coverage improves and there is less need to infill. This result is

158 evident when comparing the longer (1970-2012) versus the shorter (1993-2012)
159 analysis period (Figure 3b vs d).

160 To summarise, the following tests build our confidence in the range of
161 simulated hemispheric ratios of OHC changes: (1) hemispheric SSH 20-year trend
162 ratios are consistent between altimetry observations and CMIP simulations; (2) the
163 relationship between SSH and OHC is strong and robust for the spatial scales
164 considered (Figure 2); and (3) there is consistency between observed estimates and
165 CMIP simulations for the vertical partitioning of OHC change in the upper (0-700
166 dbar) and full depth[30] (Figure 2, S4). We note that there is likely a small positive SH
167 contribution to observed SSH trends from a salinity (freshening) driven halosteric
168 expansion[18], which may account for some of the discrepancy between SSH and OHC
169 ratios, however this has little impact on our results.

170 We can further compare observed OHC ratios by analysing not only CMIP5
171 but also CMIP3 simulations. According to models, the OHC increases are about the
172 same in both hemispheres. Thus, across all model simulations the mean ratio of SH
173 to global OHC change (0.59; Figure 4) is close to the fraction of the global ocean
174 volume for the SH (0.60). The observed ratios are smaller (0.35-0.49; Figure 4) with
175 the observational ratios largely inconsistent even when compared to each model
176 experiment mean in isolation (Figure 4, black diamonds 0.52-0.58), or to a much
177 larger composite distribution obtained from all available model simulations (633)
178 across 9 CMIP experiments (Figure S8, light grey). The resolved model-based
179 hemispheric ratio is insensitive to forcing changes, as evidenced by comparing the
180 20c3m/Historical results to the strongly forced projections (e.g. SRESA2, RCP85) that

result in enhanced ocean stratification, mixed layer shoaling and changes to ocean ventilation rates (see Supplementary Information).

Thus, it appears that our preliminary finding is robust: the SH contribution to the total upper-OHC change found in the five observational datasets is inconsistent with the CMIP model ensembles (Figures 3b, 4). The agreement between the observed and simulated SSH changes, the close correspondence between OHC and SSH (Figure 2), and the better agreement of observed and simulated OHC for the recent Argo period (with improved SH coverage) suggests systematic model biases are not the dominating factor. We thus conclude, in agreement with previous works[5-7] that long-term observational estimates of SH upper-ocean heat content change are biased low.

If models are correct in their hemispheric partitioning of OHC changes, we can use them to guide observational adjustment over the data sparse SH. Assuming that the much better sampled and more consistent estimates of observed NH OHC change (Figure S2a) are accurate, we adjust the poorly constrained SH estimates (see Methods) so that they yield an inter-hemispheric ratio that is consistent with the MMM (Figure 4). When this adjustment is applied, the various observational estimates of 35-year global upper-OHC change are substantially increased in all cases. The adjusted estimates span the range from 7.2-19.9 x 10^{22} J (Figure 5 upper inset; observed ratios 0.35-0.49 adjusted to 0.59; Figure 4), and depending on the observational analysis considered, corresponds to SH increases of 48-166%, and 24-58% increases for the global OHC (Figure 5). To provide perspective, for each observational estimate we reapply our adjustment method using the modelled ratio obtained from the distribution of simulations (Figure 4), and use a one standard

205 deviation spread to construct uncertainty bounds (Figure 5 upper inset; grey lines).
206 We note that the largest adjusted global values (Ish09[10], Lev12[11]) are consistent with
207 a recent upper-OHC change estimate[12], and if uncertainty bounds are considered this
208 agreement includes four of the five adjusted values (Figure 5 upper inset).
209 We further investigate the consistency between observations and models by
210 considering the warming for each hemisphere separately (Figure 5, lower left and
211 right bars). We consider results from CMIP3 and CMIP5 separately (Figure 5 light and
212 dark grey bars), and show the one standard deviation spread (black lines) between
213 available CMIP5 Historical (dark grey bars) and CMIP3 20c3m (light grey bars)
214 simulations. Using this measure, only two of the five observations (Dom08[8], DW10[18])
215 appear consistent with the modelled range for both hemispheres. All but one
216 observed estimate (Smi07[23]) suggest a larger NH warming than the MMM values
217 (Figure 5; left bars), and all five observed estimates show a smaller SH warming than
218 the MMM values (Figure 5; right bars). The NH modelled changes are consistent with
219 some, but not all observations, and indicate that we cannot rule out an influence of
220 model error on our adjustments.
221 Accurate estimates of global ocean warming are required to understand
222 contributions to observed sea-level and energy budget changes and to constrain
223 empirical estimates of climate sensitivity. Our analysis finds that modelled
224 hemispheric ratios of SSH changes are consistent with highly accurate altimetry
225 observations but remarkably inconsistent with in-situ based hemispheric ratios of
226 OHC changes. Adjusting the poorly constrained SH OHC change estimates to yield an
227 improved consistency with models, produces a previously unaccounted for increase
228 in global upper-OHC of 2.2-7.1 x 10^{22} J above existing estimates for 1970 to 2004

229 (Figure 5, upper inset). For perspective, these adjustments represent more than
230 double the 1970-2004 heat storage change for all non-ocean (terrestrial, cryospheric
231 and atmospheric) heat reservoirs combined[4], and highlights the importance of
232 accurately estimating ocean temperature changes. By contrasting hemispheric
233 changes in an attempt to quantify the impact of SH observation deficiencies, our
234 analysis should motivate further work to improve estimates of global OHC change.

Acknowledgements. The work of P.J.D., P.J.G. and K.E.T. from Lawrence Livermore National Laboratory is a contribution to the U.S. Department of Energy, Office of Science, Climate and Environmental Sciences Division, Regional and Global Climate Modeling Program under contract DE-AC52-07NA27344. The work of F.W.L. was performed at the Jet Propulsion Laboratory, California Institute of Technology under contract with NASA. We thank numerous colleagues from the Program for Climate Model Diagnosis and Intercomparison (PCMDI) for valuable feedback and input into this project. We also thank J. Durack of the University of California, San Francisco (USA), M. V. Durack of educAID (Australia), T. P. Boyer from the National Oceanographic Data Center, Silver Spring (USA), C. M. Domingues from the Antarctic Climate and Ecosystems CRC, Hobart (Australia), J. A Church from the Centre for Australian Weather and Climate Research, Hobart (Australia). We would like to thank the three anonymous reviewers for helpful comments on early drafts which greatly improved the manuscript. We acknowledge the sources of observed data used in this study: D. Smith and J. Murphy (Smi07), C. M. Domingues (Dom08), M. Ishii and M. Kimoto (Ish09), S. Levitus and T. Boyer (Lev12) and the International Argo Program and the national programs that contribute to it. We acknowledge the World Climate Research Programme's Working Group on Coupled Modelling, which is responsible for CMIP, and we thank the climate modelling groups (listed in Tables S1 and S2) for producing and making available their model output. For CMIP the U.S. Department of Energy's Program for Climate Model Diagnosis and Intercomparison provides coordinating support and led development of software infrastructure in partnership with the Global Organization for Earth System Science Portals. The DW10 data presented in this study can be downloaded from the CSIRO Ocean Change website at www.cmar.csiro.au/oceanchange. LLNL Release #: LLNL-JRNL-651841.

Competing Interests. The authors declare that they have no competing financial interests

Authors' Contributions. P.J.D. completed the OHC analysis, P.J.G. assisted in the OHC analysis and F.W.L completed the SSH analysis. All authors assisted with interpretation and shared responsibility for writing the manuscript.

Author Information. Correspondence and requests for materials should be addressed to P.J.D. (pauldurack@llnl.gov)

Methods Summary

We constructed near-global, interpolated maps of annual mean upper-ocean heat content (OHC) along with hemispheric timeseries for CMIP5 Historical (1970-2004), CMIP3 20c3m (1970-1999) and CMIP3/5 future model simulations (2065-2099), as well as for 5 available observations (1970-near present: Smi07[23], Dom08[8], Ish09[10], DW10[18] and Lev12[11]).

The hemispheric timeseries were computed with equal-area weighting from native model and observational grids and native land-sea masks which in most cases extend from 90°S - 90°N (Figure 3).

The mapped data is interpolated to a regular horizontal (70°S - 70°N) and vertical (0 – 700 dbar) grid for all models and observations, using an identical land-sea mask which excludes marginal seas, the Arctic Ocean and the high latitude Southern Ocean (Figure 1, S2a, S2b). After interpolation an iterative nearest neighbour infilling algorithm is employed to ensure the geographic coverage of each estimate is identical. We used a pre-computed hemispheric timeseries for the Dom08[8,21] analysis, as a gridded analysis was not available.

We contrast observed and modelled sea surface height (SSH) to assess the possible effect of model biases on our simulated OHC hemispheric totals. SSH is analysed to investigate the internal consistency between ocean warming and total steric change, and we show these quantities are highly correlated over the hemispheric scales considered (Figure 2, S4). The hemispheric contribution to global mean SSH changes in both observations and models show a strong agreement

289 (Figure 3a, c). This strong hemispheric SSH agreement provides the motivation to
290 assess modelled hemispheric OHC and compare this to observed estimates.
291 We calculate the contribution to global upper-OHC change obtained from the
292 Southern Hemisphere (SH) alone, and contrast these ratios over the analysed period
293 comparing the multi-model mean (MMM) for the CMIP5 Historical and CMIP3 20c3m
294 simulations (R; Figure 4) and observations respectively. Guided by the observed and
295 modelled consistency in SSH, we correct observations by scaling the observed
296 SH/Global ratio to match the simulated ratio of the CMIP5/3 MMM (Figure 4). This
297 technique leverages the better-sampled observed Northern Hemisphere (NH) oceans
298 and the SH/Global OHC ratio obtained from the CMIP models to provide a correction
299 term (x) for the poorly constrained SH OHC change estimate (SH_{Obs}). Once we have
300 corrected the SH OHC change estimate, we then use this (SH^{*}_{Obs}) along with the
301 existing NH OHC change estimate (NH_{Obs}) to recalculate the corrected global upper
302 OHC change total ($Global^{*}_{Obs}$) following (1-4) below:

303 $$R = \frac{SH_{Models}}{(SH_{Models} + NH_{Models})} = \frac{SH_{Obs} \times x}{((SH_{Obs} \times x) + NH_{Obs})} \quad (1)$$

304 $$x = \frac{R \times NH_{Obs}}{(1-R) \times SH_{Obs}} \quad (2)$$

305 $$SH^{*}_{Obs} = SH_{Obs} \times x \quad (3)$$

306 $$Global^{*}_{Obs} = SH^{*}_{Obs} + NH_{Obs} \quad (4)$$

307 To provide a measure of our correction uncertainty we use a one standard
308 deviation spread of the SH/Global ratio from the available simulations (Figure 4).
309 These are used to generate representative uncertainty bars for our global upper-

OHC estimates (Figure 5; upper inset, grey bars). We note that this provides a simplified uncertainty estimate, however due to the large number of observational and model simulations used in the study a more complex treatment was not undertaken.

To enhance the model ensemble sample size, CMIP3 20c3m (1970-1999) simulations and CMIP3 and CMIP5 future projections (2050-2099; SRES & RCPs) are also sampled to assess the potential role of forcing on hemispheric ratios. Model drift was not explicitly corrected, as drift is primarily an issue in the deeper ocean (>2000 dbar) and correction considerably reduced the number of available simulations. Instead, we calculated the impact of drift correction on a specific sub-suite of the CMIP5 Historical simulations (Figure S10, S11). We found that for the drift-corrected models this changed the MMM ratios by a negligible amount (<2%) and therefore the hemispheric analysis was found to be insensitive to drift correction. The full-depth analysis which compares OHC change to total steric changes (Figure 2, panels D, E, F) required drift-correction, which accounts for spurious deep ocean anomalies, and due to limited data availability reduced available simulations from 171 to 100 (Figure 2).

For more detailed descriptions and supporting figures please refer to the Supplementary Information. tNŜLJI·NŜŘ ōè [[b[dzyŘŜN /2yűNI·Ŏű 59π ! /рнплтb !нтоппф

References

1 Levitus, S., Antonov, J. & Boyer, T. Warming of the world ocean, 1955–2003. *Geophys Res Lett* **32**, L02604, doi:10.1029/2004GL021592 (2005).

2 Church, J. A. *et al.* Revisiting the Earth's sea-level and energy budgets from 1961 to 2008. *Geophys Res Lett* **38**, L18601, doi:10.1029/2011GL048794 (2011).

3 Otto, A. *et al.* Energy budget constraints on climate response. *Nature Geosci* **6**, 415-416, doi:10.1038/ngeo1836 (2013).

4 Rhein, M. *et al.* in *Climate Change 2013: The Physical Science Basis. Contribution of Working Group I to the Fifth Assessment Report of the Intergovernmental Panel on Climate Change* (eds T. F. Stocker *et al.*) Ch. 3, 255-315 (Cambridge University Press, 2013).

5 Gregory, J. M., Banks, H. T., Stott, P. A., Lowe, J. A. & Palmer, M. D. Simulated and observed decadal variability in ocean heat content. *Geophys Res Lett* **31**, L15312, doi:10.1029/2004GL020258 (2004).

6 Gouretski, V. & Koltermann, K. P. How much is the ocean really warming? *Geophys Res Lett* **34**, L01610, doi:10.1029/2006GL027834 (2007).

7 Gille, S. T. Decadal-Scale Temperature Trends in the Southern Hemisphere Ocean. *Journal of Climate* **21**, 4749-4765, doi:10.1175/2008JCLI2131.1 (2008).

8 Domingues, C. M. *et al.* Improved estimates of upper-ocean warming and multi-decadal sea-level rise. *Nature* **453**, 1090-1093, doi:10.1038/nature07080 (2008).

9 Lyman, J. M. & Johnson, G. C. Estimating Annual Global Upper-Ocean Heat Content Anomalies despite Irregular In Situ Ocean Sampling*. *Journal of Climate* **21**, 5629-5641, doi:10.1175/2008JCLI2259.1 (2008).

10 Ishii, M. & Kimoto, M. Reevaluation of historical ocean heat content variations with time-varying XBT and MBT depth bias corrections. *Journal of Oceanography* **65**, 287-299, doi:10.1007/s10872-009-0027-7 (2009).

11 Levitus, S. *et al.* World ocean heat content and thermosteric sea level change (0–2000m), 1955–2010. *Geophys Res Lett* **39**, L10603, doi:10.1029/2012GL051106 (2012).

12 Lyman, J. M. & Johnson, G. C. Estimating Global Ocean Heat Content Changes in the Upper 1800 m since 1950 and the Influence of Climatology Choice*. *Journal of Climate* **27**, 1945-1957, doi:10.1175/JCLI-D-12-00752.1 (2014).

13 Wijffels, S. E. *et al.* Changing Expendable Bathythermograph Fall Rates and Their Impact on Estimates of Thermosteric Sea Level Rise. *Journal of Climate* **21**, 5657-5672, doi:10.1175/2008JCLI2290.1 (2008).

14 Cowley, R., Wijffels, S., Cheng, L., Boyer, T. & Kizu, S. Biases in Expendable Bathythermograph Data: A New View Based on Historical Side-by-Side Comparisons. *Journal of Atmospheric and Oceanic Technology* **30**, 1195-1225, doi:10.1175/JTECH-D-12-00127.1 (2013).

15 Gille, S. T. Warming of the Southern Ocean Since the 1950s. *Science* **295**, 1275-1277, doi:10.1126/science.1065863 (2002).

16 Aoki, S., Bindoff, N. L. & Church, J. A. Interdecadal water mass changes in the Southern Ocean between 30°E and 160°E. *Geophys Res Lett* **32**, L07607, doi:10.1029/2004GL022220 (2005).

17 Alory, G., Wijffels, S. & Meyers, G. Observed temperature trends in the Indian Ocean over 1960–1999 and associated mechanisms. *Geophys Res Lett* **34**, L02606, doi:10.1029/2006GL028044 (2007).

18 Durack, P. J. & Wijffels, S. E. Fifty-Year Trends in Global Ocean Salinities and Their Relationship to Broad-Scale Warming. *Journal of Climate* **23**, 4342-4362, doi:10.1175/2010JCLI3377.1 (2010).
19 Barnett, T. P. *et al.* Penetration of Human-Induced Warming into the World's Oceans. *Science* **309**, 284-287, doi:10.1126/science.1112418 (2005).
20 AchutaRao, K. M. *et al.* Variability of ocean heat uptake: Reconciling observations and models. *Journal of Geophysical Research: Oceans* **111**, C05019, doi:10.1029/2005JC003136 (2006).
21 Gleckler, P. J. *et al.* Human-induced global ocean warming on multidecadal timescales. *Nature Clim. Change* **2**, 524-529, doi:10.1038/nclimate1553 (2012).
22 Pierce, D. W., Gleckler, P. J., Barnett, T. P., Santer, B. D. & Durack, P. J. The fingerprint of human-induced changes in the ocean's salinity and temperature fields. *Geophys Res Lett* **39**, L21704, doi:10.1029/2012GL053389 (2012).
23 Smith, D. M. & Murphy, J. M. An objective ocean temperature and salinity analysis using covariances from a global climate model. *Journal of Geophysical Research: Oceans* **112**, C02022, doi:10.1029/2005JC003172 (2007).
24 Banks, H. T. & Gregory, J. M. Mechanisms of ocean heat uptake in a coupled climate model and the implications for tracer based predictions of ocean heat uptake. *Geophys Res Lett* **33**, L07608, doi:10.1029/2005GL025352 (2006).
25 Fyfe, J. C. Southern Ocean warming due to human influence. *Geophys Res Lett* **33**, L19701, doi:10.1029/2006GL027247 (2006).
26 Talley, L. D. Shallow, Intermediate, and Deep Overturning Components of the Global Heat Budget. *Journal of Physical Oceanography* **33**, 530-560, doi:10.1175/1520-0485(2003)033<0530:SIADOC>2.0.CO;2 (2003).
27 Church, J. A. *et al.* in *Climate Change 2013: The Physical Science Basis. Contribution of Working Group I to the Fifth Assessment Report of the Intergovernmental Panel on Climate Change* (eds T. F. Stocker *et al.*) Ch. 13, 1137-1216 (Cambridge University Press, 2013).
28 Church, J. A., White, N. J., Coleman, R., Lambeck, K. & Mitrovica, J. X. Estimates of the Regional Distribution of Sea Level Rise over the 1950–2000 Period. *Journal of Climate* **17**, 2609-2625, doi:10.1175/1520-0442(2004)017<2609:EOTRDO>2.0.CO;2 (2004).
29 Roemmich, D. & Gilson, J. The 2004-2008 mean and annual cycle of temperature, salinity, and steric height in the global ocean from the Argo Program. *Prog Oceanogr* **82**, 81-100, doi:10.1016/j.pocean.2009.03.004 (2009).
30 Flato, G. *et al.* in *Climate Change 2013: The Physical Science Basis. Contribution of Working Group I to the Fifth Assessment Report of the Intergovernmental Panel on Climate Change* (eds T. F. Stocker *et al.*) Ch. 9, 741-866 (Cambridge University Press, 2013).

Figures

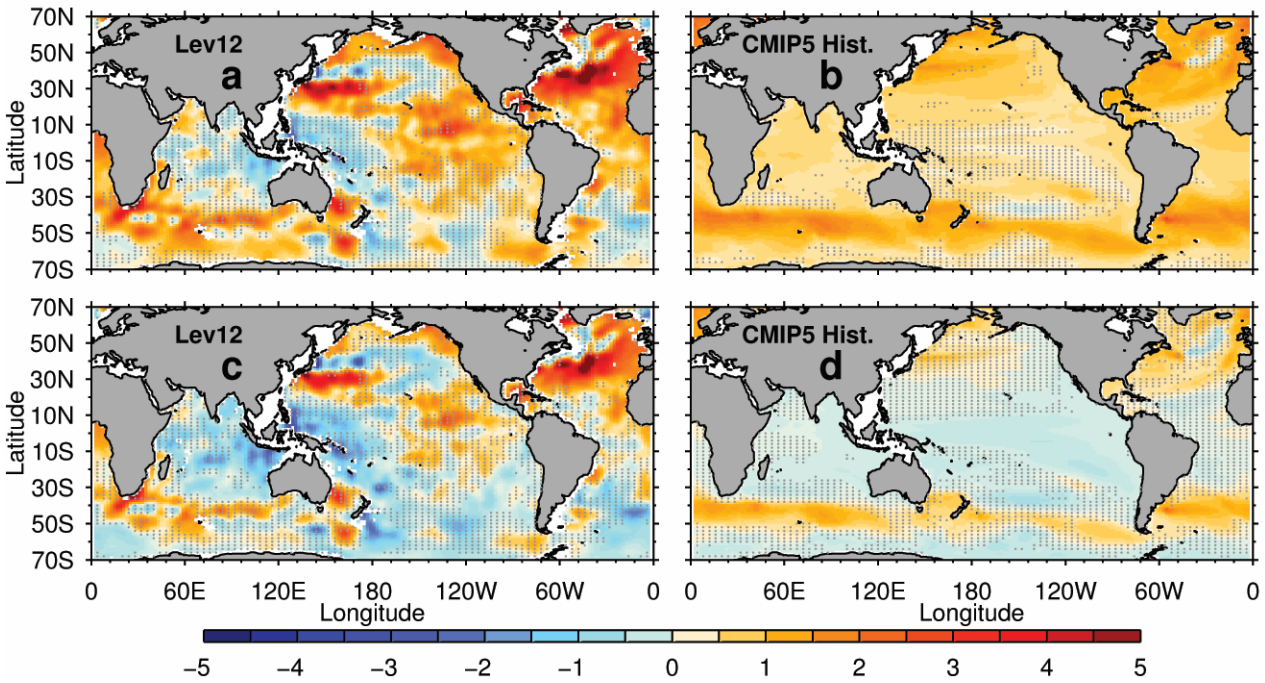

FIG. 1. **Upper-ocean (0-700 dbar) heat content trends for 1970-2004.** Observations (a and c) are from Lev12[11]. The multi-model mean (MMM) results (b and d) are from CMIP5 "Historical" simulations. Lower panels (c and d) show maps with the global mean trends removed. All trends are reported in units of J x 10^3 kg^{-1} $35yrs^{-1}$ (4 ≈ 1°C $35yrs^{-1}$ depth averaged warming). Stippling marks regions where the 4 observational estimates do not agree in sign (panels a and c) or where <75% of the models simulate trends with a sign opposite to the MMM (panels b and d). Maps for the alternative observational estimates and for several additional CMIP experiments are shown in Figures S2a and S2b respectively.

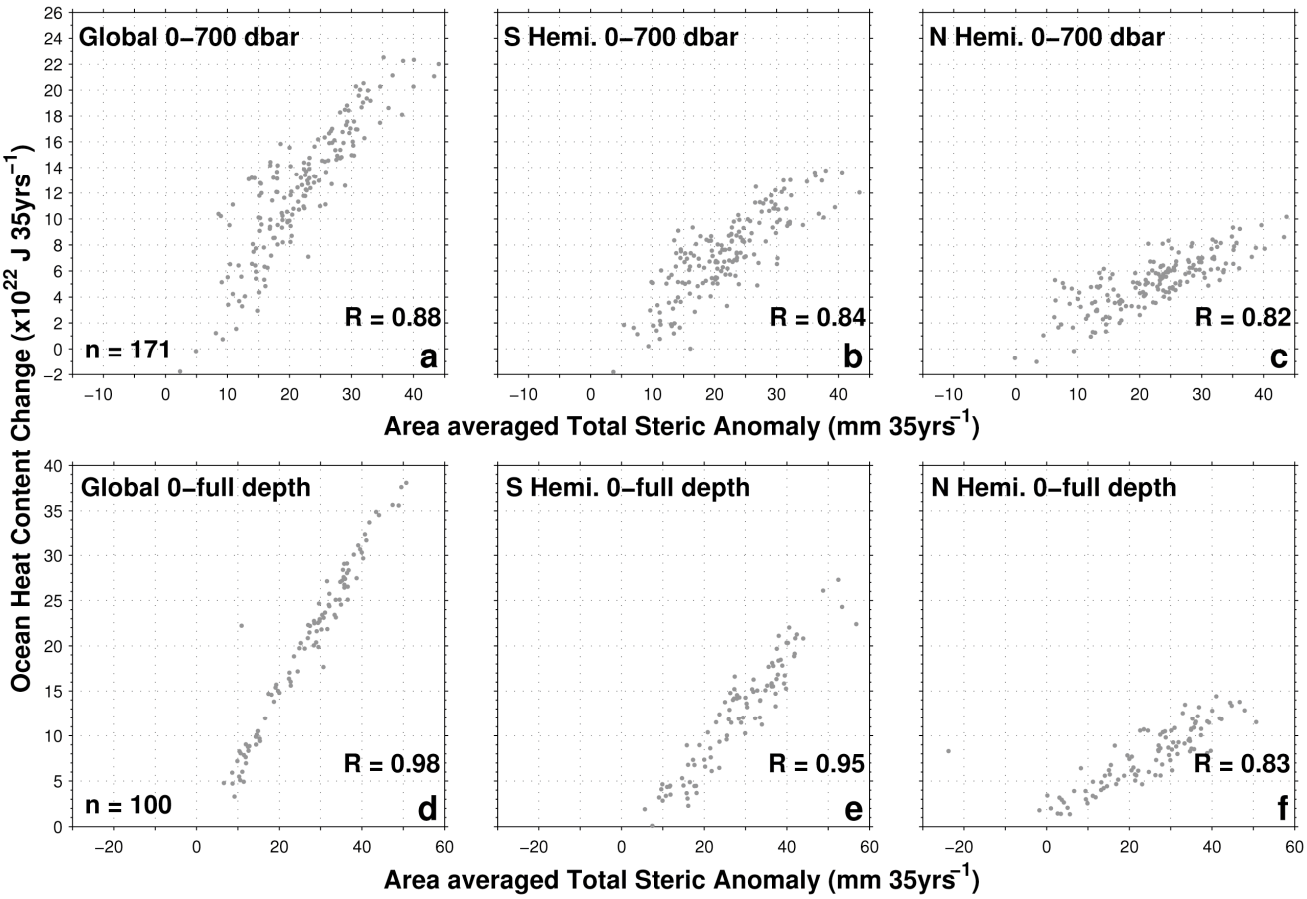

FIG. 2. **Global and hemispheric OHC compared to total steric anomalies simulated by models for 1970-2004.** The CMIP5 "Historical" volume-integrated 35-year trends in OHC change are plotted against area weighted average total steric anomalies (equivalent to sea surface height [SSH]) for the upper 700 dbar in upper panels (a, b, c) and for the full depth ocean in the lower panels (d, e, f). The full depth ocean analysis requires drift correction and consequently fewer models were assessed.

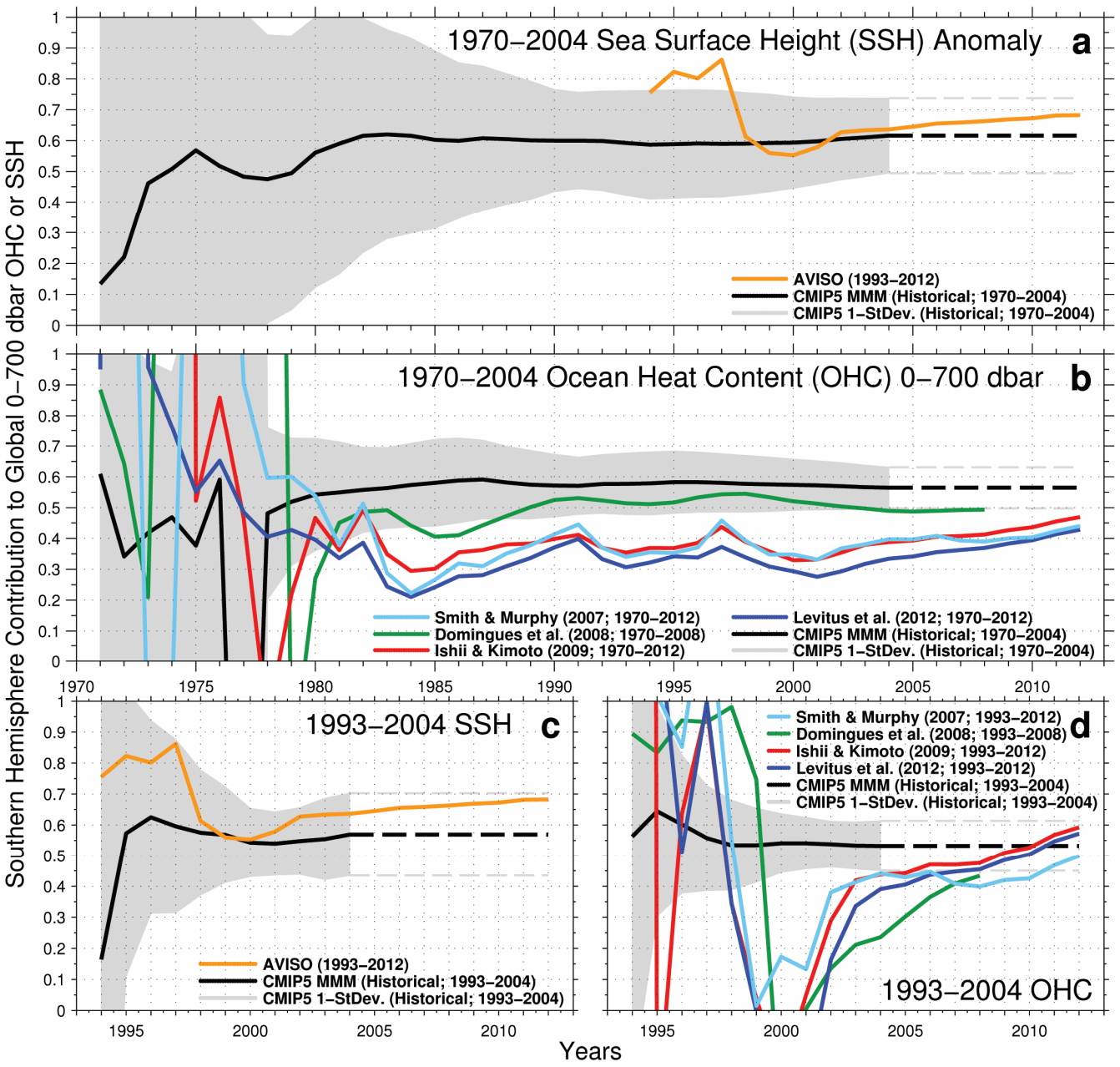

FIG. 3. **Southern Hemisphere fractional contributions to global upper-OHC or global SSH anomaly for varying trend lengths (1-35 years).** Panels a (SSH) and b (OHC) show results over 1-35-years (1970-2004). Panels c (SSH) and d (OHC) show results for a shorter 11-year period (1993-2004) for which observed SSH data is available. Observed results extend to 2012 if available. Discontinuous black and grey lines extend 2004 CMIP5 values to 2012. The CMIP5 MMM and 1 standard deviation spread are obtained from CMIP5 "Historical" simulations.

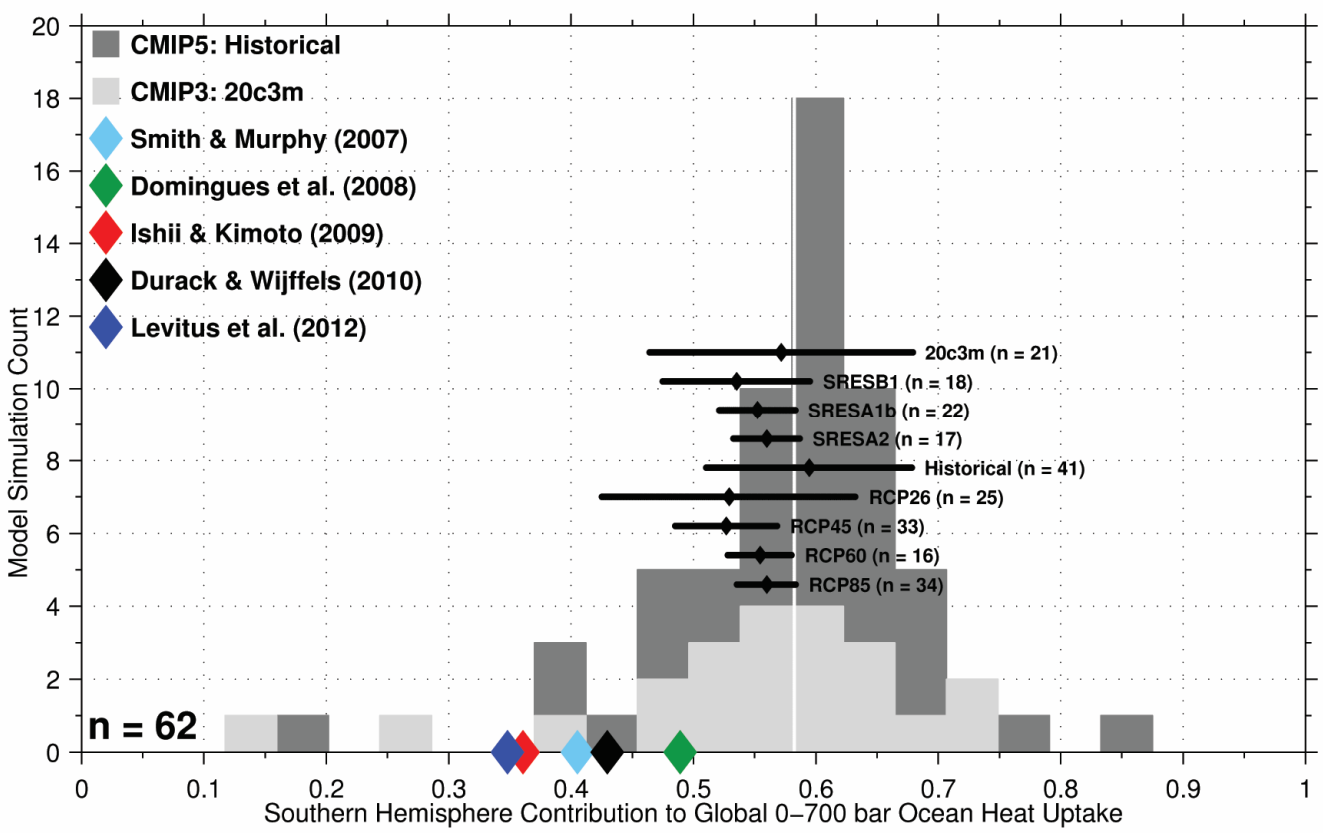

FIG. 4. **Histogram of the observed and simulated Southern Hemisphere contribution to global OHC trends for 1970-2004.** The distribution from 62 independent CMIP5 (Historical) and CMIP3 (20c3m) model means (average of single model simulations) is shown in dark grey (21 20c3m CMIP3; overlaid light grey). Results from additional CMIP experiments are summarised with the MMM and one standard deviation spread indicated by small black diamonds and horizontal black lines respectively. The full ensemble MMM (dark grey) is presented as a vertical white line. Figure S8 shows composite single simulation distributions and S9 shows each CMIP experiment. Models are listed in Tables S1 and S2.

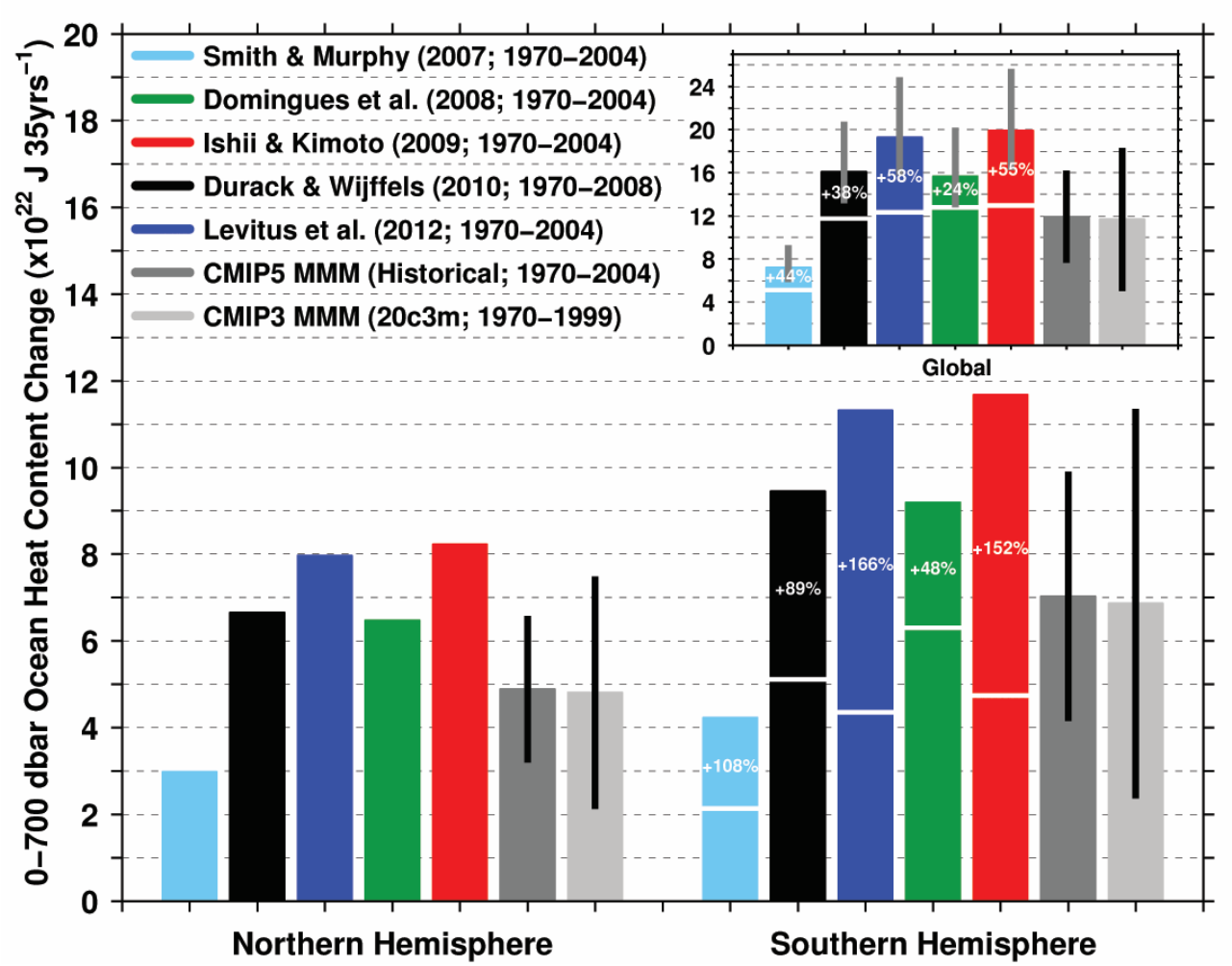

FIG. 5. **Observed and simulated hemispheric and global upper-ocean (0-700 dbar) heat content change for 1970-2004.** For the SH and global results horizontal white lines indicate the original unadjusted changes. Full bars indicate the adjusted values, which are revised so that hemispheric ratios of heat uptake match the multi-model mean (MMM) results from CMIP5 Historical and CMIP3 20c3m simulations (Figure 4). The NH and adjusted SH estimates are summed to yield global estimates (upper inset). Uncertainty estimates show the range of adjusted values obtained using the one standard deviation spread of model-simulated ratios (Figure 4) and are indicated by vertical grey lines. The one standard deviation spread in simulated estimates for CMIP5 and CMIP3 is indicated by black lines.